

Small Molecule Compound DHPA Screened by Computer-Aided Drug Design and Molecular Dynamics Simulation Inhibits Neuroblastoma Cell Proliferation by Targeting TrkB

Tianyi Liu,^{||} Hongli Yin,^{||} Qingyang Hu,^{||} Xue Dong, Bin Xin, Yue Wu, Xuejiao Hu, Wenxin Yan, and Zhong Li*



Cite This: *ACS Omega* 2024, 9, 42227–42244

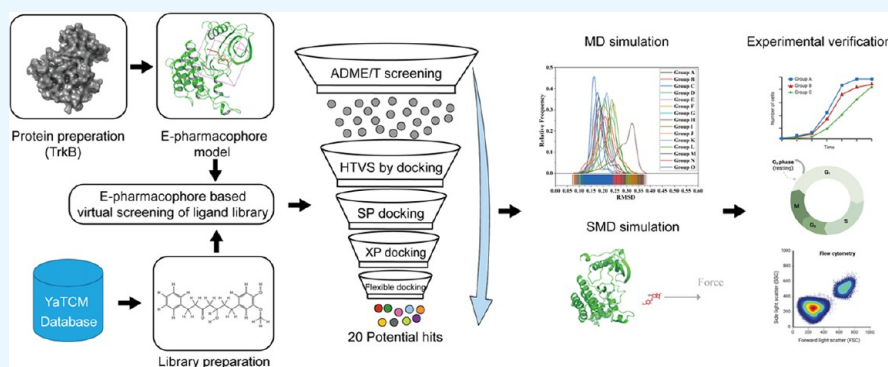


Read Online

ACCESS |

Metrics & More

Article Recommendations



ABSTRACT: Neuroblastoma (NB) is a rare and malignant pediatric solid tumor. Due to its heterogeneity, it poses significant challenges for treatment, resulting in a high mortality rate. This study aimed to identify new therapeutic drugs by modeling the TrkB receptor from PDB 4AT5 and conducting virtual screening of compounds from the YaTCM database (containing 47,696 compounds derived from 6220 Traditional Chinese Medicines). The screening utilized the E-pharmacophore approach to select compounds with potential binding affinity to TrkB. The binding abilities of these compounds were tested through molecular dynamics simulations, stretch dynamics simulations, and US simulations. Among the top 11 optimized hit compounds, DHPA and 3''-demethylhexahydrocurcumin are prominent. Further simulations reveal that they form stable receptor–ligand binary complexes with TrkB. In subsequent in vitro cell experiments, 3''-demethylhexahydrocurcumin is eliminated due to its high IC₅₀ for killing NB cells. Low concentrations of DHPA can significantly kill NB cells. Additionally, DHPA can inhibit the expression of TrkB, the activation of TrkB's downstream signaling pathways, and affect the thermal stability of TrkB protein and its response to streptase protease degradation. DHPA may be a potential TrkB inhibitor.

INTRODUCTION

Neuroblastoma (NB) is an extremely rare and highly malignant solid tumor in children, and is known as the “king of childhood tumors”.¹ It can involve multiple parts of the body, most commonly in the adrenal glands, neck, chest, abdomen, and pelvis. Due to the unique tumor gene composition and biological behavior of each patient, this leads to tumor heterogeneity.² Tumor cells may naturally regress from an undifferentiated malignant state or differentiate into benign cells; or after receiving combined treatment with high-intensity and multiple means (such as chemotherapy, radiotherapy, surgery, autologous peripheral blood stem cell transplantation, etc.), the disease progression or recurrence still cannot be controlled.³ In addition to the troublesome heterogeneity problem, the resistance of tumor cells to chemotherapy and radiotherapy, the metastasis and recurrence

of the tumor, and other difficulties have also brought many challenges to the treatment of NB.⁴ To address these issues, the current focus of research is to find the commonalities of different types of NB, and actively explore new treatment strategies, such as immunotherapy, targeted therapy, and personalized treatment.

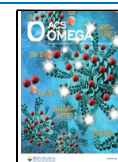
The neurotrophic receptor tyrosine kinase (NTRK) gene encodes neurotrophic factor receptors, which are closely related to cell growth, differentiation, and survival. The

Received: May 13, 2024

Revised: September 20, 2024

Accepted: September 26, 2024

Published: October 4, 2024



NTRK gene family includes NTRK1, NTRK2, and NTRK3, among which NTRK2 (encoding TrkB) has the closest relationship with NB. The activation of the tropomyosin receptor kinase B (TrkB) receptor is associated with various biological processes in NB, including cell survival, proliferation, and migration. The activation of the TrkB signaling pathway, especially through the PI3K/AKT and MAPK pathways, is considered to play a key role in the development and progression of NB.⁵ These studies show that TrkB may be a potential target for the treatment of NB. The development of drugs targeting it has become a hotspot in the field of pediatric NB research currently. Currently, there are already inhibitors targeting NTRK fusion genes on the market, such as Larotrectinib⁶ (Vitrakvi) and Entrectinib⁷ (Rozlytrek), etc.

Our research is focused on discovering novel TrkB inhibitors from the extensive natural product library of Traditional Chinese Medicine (TCM) to explore their potential in treating NB. Utilizing advanced technologies such as computer-aided drug design (CADD), molecular docking, molecular dynamics (MD) simulations, stretching molecular dynamics (SMD) simulation, and umbrella sampling (US), we have identified a promising small molecule compound. This compound, named 5-hydroxy-7-(4-hydroxy-3-methoxyphenyl)-1-phenylheptan-3-one (DHPA), is derived from the rhizome of TCM herb *Alpinia officinarum* Hance. The selection process involved a comprehensive screening and evaluation methodology. Initially, the CADD approach facilitated the identification of potential TrkB inhibitors by predicting their binding affinity toward the TrkB receptor. Subsequently, molecular docking studies provided insights into the binding modes and interactions between DHPA and the TrkB receptor, highlighting the compound's potential inhibitory effects. To further validate these findings, MD simulations and SMD simulation were employed to assess the stability of the TrkB-DHPA complex, ensuring the compound's effective binding over time. US techniques were then used to calculate the free energy profiles, which provides the dissociation energy of DHPA to TrkB.

Alpinia officinarum Hance is a highly regarded medicinal plant in the field of TCM, containing a rich variety of active ingredients.⁸ The diarylheptanoid extracted from *Alpinia officinarum* Hance exhibits many powerful biological activities, including anticancer, antibacterial, anti-inflammatory, antioxidant, and other multiple functions.^{8–10} DHPA is one of the five diarylheptanoid compounds in the rhizome of *Alpinia officinarum*, and its chemical structure was determined in the early 21st century.¹¹ Current research has clearly shown that DHPA has the ability to inhibit pancreatic lipase, resist *Helicobacter pylori* and tuberculosis, and also exhibit antioxidant and anti-inflammatory properties.^{10–12} However, the role of DHPA in the treatment of NB has not been studied.

The hit compound DHPA is derived from *Alpinia officinarum* and has a unique structure. This compound shows a certain degree of inhibitory activity against the TrkB receptor, which may in a sense imply its potential possibility in the field of NB treatment. This research provides assistance to some extent in exploring new TrkB inhibitors from TCM. At the same time, it also shows the integration of traditional medicine and modern drug discovery and computational biology techniques within a specific range. Our discovery has opened up some ideas for further development and optimization of DHPA to make it a new treatment option

for NB and has a certain potential for improving efficacy through the TrkB pathway.

METHODS

CADD. Preparation of Protein. The crystal structure of TrkB (4AT5)¹³ was retrieved from the Protein Data Bank (PDB). The structure of TrkB in the PDB database was refined and improved using the Maestro 13.5 Protein Preparation module.¹⁴ Specifically, correct bond orders were assigned, water molecules and other nonspecific chemical components were omitted from the crystal structure, and hydrogen atoms were added to the protein structure to remold the conformational isomers and ionization states of amino acid residues, and missing side chains and loop regions were supplemented. The OPLS4 force field was used to constrain energy minimization of the TrkB structure, achieving high-precision hydrogen atom addition and hydrogen bond optimization. The Maestro 13.5 Protein Grid Generation module was used to prepare the docking grid with the TrkB inhibitor GW2580 as the reference ligand. The boundary box for docking was set to a range of 20 Å × 20 Å × 20 Å around GW2580.

Ligand Preparation. The natural product database of TCM (YaTCM)¹⁵ developed by Nankai University was used to mine Chinese medicinal compounds. The YaTCM database collects 47,696 natural products from 6220 kinds of TCM, serving as the ligand library for this study. The LigPrep module¹⁶ of Maestro 13.5 was used to prepare the database by adjusting the twist of the ligands and assigning protonation states. Subsequently, hydrogen atoms were added to generate stereoisomers and determine ionization states, thereby optimizing the three-dimensional (3D) structures of the ligands. Additionally, the OPLS4 force field was used for energy minimization and optimization of the low-energy 3D structures of the ligands. After preprocessing, 58,048 prescreened compounds were obtained as the ligand library. The QikProp module of Maestro 13.5 was used to conduct the first round of screening based on the drug-like rules “Lipinski Ro5”, “Verber Ro3”, resulting in 22,227 hit compounds that met the criteria.

Virtual Screening by Molecular Docking. First, a high-throughput virtual screening (HTVS) was performed on the 22,227 compounds library screened in the previous step against the target TrkB, and the top 20% compounds with the highest scores were extracted according to the Glide Grid module of Maestro 13.5. Subsequently, a standard precision (SP) was conducted, and the screened compounds were ranked again based on the Glide Score, and the top 20% compounds with the highest scores were extracted. Finally, an extra precision (XP) was performed, and the top 20% compounds with the highest scores were retained according to the Glide Grid module of Maestro 13.5. A third round of screening was conducted based on flexible docking, and flexible docking was performed for the compounds screened in the previous step to select the final hit compounds that could bind well to TrkB.

Toxicity Prediction. The hepatotoxicity, nephrotoxicity, acute oral toxicity, and Ames mutagenicity of the hit compounds were predicted using admetSAR,¹⁷ and the hit compounds with greater toxic side effects were removed.

Binding Mode Analysis of Hit Compounds with the Target Protein. The binding mode between the hit compounds and the target protein was analyzed using the two-dimensional (2D) Sketcher module of Maestro 13.5

software, including the amino acid residues related to the hit compounds, hydrogen bonds, hydrophobic interactions, halogen bonds, and nonbond interactions such as HB, pi stacking, and cation-pi, with a cut-off value set at 5.0.

MD Simulation. Building a Topological Structure Model of the Protein–Ligand System. The MD simulation was conducted using GROMACS (2023.1) on an Ubuntu 20.04.01 platform, equipped with an Intel Core i9–13900k CPU and GeForce RTX 4070Ti Super all within a Dell T3660 workstation. We obtained five different TrkB structures from the PDB database, namely, 4AT5, 4AT4, 4AT3, 4ASZ, and 4FOI.¹³ For each hit compound, a total of 15 MD simulations were carried out randomly 3 times with these five different TrkB structures, respectively. Because in GROMACS, the initial velocities of molecules are usually calculated based on the Maxwell–Boltzmann distribution. This distribution describes the velocity distribution of molecules in the thermal equilibrium state. GROMACS will calculate the average velocity and variance of each molecule according to the simulated temperature and the mass of the molecule. Then, it will randomly draw a velocity value from this distribution as the initial velocity of the molecule. The initial velocity of each molecule is random. The repetitive experiments with different TrkB structures and different random initial velocities are to meet the requirements of minimum robustness and reduce the bias caused by systematic errors.

Initially, the heavy atoms and small molecules of the proteins were modified using the SPDBV 4.10 software.¹⁸ Next, the topology structure of the protein was calculated using the AMBER99SB-ILDN force field, while the topology structure of the ligand was determined using the AMBER force field in combination with the Acpype online tool (<http://bio2byte.be/acpype/>).^{19,20} Simulation system parameter settings: The complex was solved in TIP3P water model and immersed in a cube box extending to at least 1 nm of the solved on all sides. Neutralization of the system was achieved through the addition of Na⁺ and Cl[−] ions, followed by further supplementation with 0.15 M NaCl, bringing the system to a near-physiological state. Energy minimization: Subsequently, the steepest descent algorithm was applied for 5000 steps to perform energy minimization, achieving a maximum force below 1000 kJ/mol/nm. The system was then subjected to constrained number of particles, volume, temperature (NVT) and number of particles, pressure, temperature (NPT) equilibration for 100 ps, ensuring a well-equilibrated and stable system at 310 K and 1 bar. MD simulation: The MD simulation of the complex lasted for 60 ns, encompassing a total of 30 million steps. During the simulation, the Verlet cut-off scheme and Leap-frog integrator were employed with a step size of 2 fs, and trajectory data was saved every 10 ps. Periodic boundary conditions were introduced during the simulation to eliminate boundary effects caused by limitations in the scale of the simulated system.

Molecular Mechanics Poisson–Boltzmann Surface Area (MM/PBSA) Method Is a Common Approach for Estimating the Stability of Protein–Ligand Complexes.²¹ This method estimates the free energy change of the complex using MD simulation trajectories, which typically includes electrostatic potential energy, van der Waals forces, and solvation free energy contributions. In this study, gmx-MM/PBSA 1.6.1^{22,23} was used to calculate the MM/PBSA binding free energy of protein–ligand complexes. We analyzed the energy contributions from ΔE_{ele} , ΔE_{vdW} , ΔG_{solv} and other factors to assess the affinity between the target and the compound. The MD

simulation trajectories from 30 to 60 ns were exploited to calculate the binding free energy of the complex. The representation of the binding free energy (ΔG_{bind}) of the protein–ligand complexes was calculated using the following formula

$$\Delta G_{\text{bind}} = G_{\text{complex}} - (G_{\text{protein}} + G_{\text{ligand}}) \quad (1)$$

$$\Delta G_{\text{bind}} = \Delta E_{\text{MM}} + \Delta G_{\text{solv}} - T\Delta S \quad (2)$$

$$\Delta E_{\text{MM}} = \Delta E_{\text{vdW}} + \Delta E_{\text{ele}} \quad (3)$$

$$\Delta E_{\text{bind}} = \Delta E_{\text{vdW}} + \Delta E_{\text{ele}} + \Delta G_{\text{solv}} - T\Delta S \quad (4)$$

ΔE_{MM} is the gas-phase interaction energy; ΔG_{solv} is the solvation free energy, and $T\Delta S$ represents the change in conformational entropy. Among them, ΔE_{MM} includes ΔE_{ele} and ΔE_{vdW} , and ΔG_{solv} is the interaction energy between solvent molecules and protein and ligand molecules, which can affect the binding free energy. In this study, due to the high computational cost and low prediction accuracy of the change in conformational Entropy ($T\Delta S$), it was not considered here.²⁴

Root-Mean-Square Deviation (RMSD) of MD Simulation Trajectories Reflects the Subtle Variations in the Spatial Conformational Fluctuations of Protein–Ligand Complexes at Different Time Points.²⁵ The shorter the time required to reach equilibrium and the smaller the amplitude of the RMSD at the equilibrium state, the greater the stability of protein–ligand complex binding. To this end, in our study, we utilized the “gmx rms” command to compute RMSD. We employed least-squares superposition with the backbone selected as the output group for RMSD calculations.²⁶

Root Mean Square Fluctuation (RMSF) Embodies the Degree of Fluctuation Exhibited by a Protein Structure during the Simulation Process. Through MD simulation, the root-mean-square value of the displacement of different amino acid residues relative to their average position within the simulation time can be computed. A lower RMSF value indicates that the protein structure at the corresponding position is more stable during the simulation with less fluctuation. Conversely, a higher RMSF value signifies greater fluctuation of the protein structure. In the design process of small molecule inhibitors, key amino acids play a crucial role in the binding stability of the complex. In this study, we screened out better compounds based on the fluctuation of amino acids in the hinge region and DFG region of the TrkB protein by the hit compounds. In this research, the “gmx rmsf” command is employed to calculate the RMSF of amino acid residues.

Free Energy Landscape (FEL) of Receptor–Ligand Complex Provides a Vivid and Informative Two-or Three-Dimensional Depiction of the Changes in Free Energy That Occur during the Binding Process. The investigation of FEL holds great value in various interdisciplinary fields. This study aims to evaluate the affinity and binding stability of receptor–ligand complexes by analyzing the FEL of receptor–ligand complex. The translational and rotational motion of the MD simulation trajectory is corrected using the gmx trjconv module. The FEL of protein–ligand complex stability is calculated using the gmx sham module within the time range of 30–60 ns. The gmx trjconv module is used to extract the conformation of the energy minimum point after analyzing the energy well. The binding mode of the lowest energy conformation in the energy well is analyzed using the 2D

Sketcher module in Maestro 13.5 software, and a 3D FEL graph is created using ORIGIN 2021. The formula for calculating FEL can reflect the various interactions and dynamic changes between the receptor and ligand molecules.^{27,28} The result of FEL is calculated using the following formula

$$G_i = -k_B T \ln(N_i/N_{\max}) \quad (5)$$

k_B is Boltzmann's constant, T is the absolute temperature, N_i is the probability density in MD data, and N_{\max} represents the maximum probability density in MD data.

SMD Simulation and US. The relaxed conformations obtained from the solvation system and NPT simulations were used as the starting structures for the SMD simulations. Then, the pulling code of GROMACS was used to transform the ligand into the displaced state, and a harmonic force with a cantilever spring constant of $k = 300$ kJ/mol·nm² was applied at the centroid of the ligand. The pulling speed was $v = 0.01$ nm/ps, and the stretching direction was along the positive X -axis. During the SMD simulation, the system coordinates were recorded every 0.1 ps. As the ligand moved along the positive X -axis, the conformations of the TrkB- the hit compounds system and the harmonic spring force varying with displacement were extracted. The structure of TrkB- the hit compounds was recorded at every step of approximately 0.2 nm, serving as the starting shape for the US evaluation. Along the dissociation path, an appropriate number of TrkB- the hit compounds shapes were released from the bound state to the unbound state. A short NPT simulation with an interval of 0.1 ns was performed first to relax the system, followed by an US simulation of 10 ns. Finally, these simulations were integrated using the weighted histogram method to calculate the energy change during the traction process.²⁹

Cell Culture. The NB cell line SK-N-BE(2) was cultured in DMEM/F-12 (BC-M-002, Biochannel, China). SK-N-SH was cultured in α -MEM (BC-M-042, Biochannel, China). KELLY was cultured in RPMI 1640 (BC-M-017, Biochannel, China). To the above-mentioned media, 10% heat-inactivated fetal bovine serum (BC-SE-FBS06, Biochannel, China) and 1% penicillin-streptomycin (C0222, Beyotime, China) were added. The cells were cultured in a humidified incubator with 5% CO₂ at 37 °C, and mycoplasma contamination was regularly detected. The above-mentioned cell lines were purchased from the National Collection of Authenticated Cell Cultures (Shanghai, China) within the past 5 years.

Cell Proliferation and Viability Assays. A total of 1×10^4 NB cell lines SK-N-BE(2) per 200 μ L were seeded in 96-well plates and incubated overnight at 37 °C. Subsequently, the cells were treated with gradient concentrations (from 1 to 200 μ g/mL) of DHPA (CFN95135, ChemFaces, China) or 3'-demethylhexahydrocurcumin(R2849, NatureWill, China) and incubated for another 48 h. The control group was treated with an equal volume of DMSO (final DMSO volume <0.1% of the cell culture medium (v/v), and toxicity <0.1%). Cell viability was measured using the CCK-8 assay (Dojindo Molecular Technologies, MD). The relative survival rate of NB cells treated with DHPA or 3'-Demethylhexahydrocurcumin was calculated using GraphPad Prism 10.0.2. Each drug concentration treatment was repeated 3 times, and the background readings from each well of the medium were subtracted to standardize the results.

Colony Formation Assay. NB cell lines SK-N-BE(2) treated with DHPA at the indicated concentrations were

inoculated at a density of 2000 per well in six-well plates and cultured for approximately 1 week. The media was discarded after the culture, rinsed 3 times with cool, sterile PBS, preserved with 4% formaldehyde, and stained with 0.1% crystal violet. The number of colonies was then counted macroscopically.

CETSA. NB cell lines SK-N-BE(2) were incubated with DMSO or 10 μ g/mL of DHPA for 1 h and washed with PBS 3 times. Then, the cells were suspended in 1 mL of RIPA buffer and divided into equal volumes, followed by heating for 3 min at the indicated temperatures (50, 55, 60, 65 °C). After heating, three snap freeze–thaw cycles were applied to lyse the cells, and then the Western blotting experiment was performed as previously described.

DARTS. NB cell lines SK-N-BE(2) were collected and lysed with RIPA buffer (P0013C, Beyotime, China) containing protease inhibitor Cocktail (C0001, TargetMol, China) and phosphatase inhibitors Cocktail II(C0003, TargetMol, China). Then, the lysis buffer was supplemented with TNC buffer. The lysates were aliquoted into 1.5 mL tubes and incubated overnight in a refrigerator at 4 °C with DMSO or 10 μ g/mL of DHPA. After incubation, the lysates were digested with 1 μ g of Pronase for every 100 μ g of lysate for exactly 15 min. Then, protein loading buffer was added immediately, and the lysates were heated to stop proteolysis. Western blot analysis was performed for further analysis.

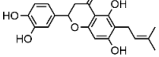
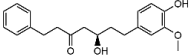
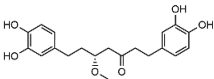
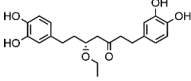
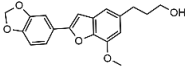
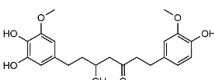
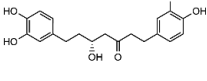
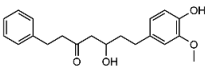
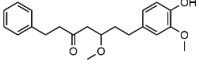
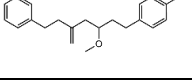
Cell Apoptosis and Cell Cycle Analysis. For apoptosis analysis, NB cell lines SK-N-BE(2) were extracted using a trypsin solution devoid of EDTA, washed, and stained with an Annexin V-FITC kit (Miltenyi Biotec). For cell cycle analysis, the cells were removed, subsequently washed, and then preserved in ice-cold 70% ethanol at 4 °C overnight. The following day, cells were stained with propidium iodide/RNase A staining solution (Sigma-Aldrich) for 20 min at room temperature. Flow cytometry was used to examine the samples (Beckman Gallios, Germany), and cell cycle distribution was analyzed using FlowJo v10 (Tree Star) software.

Western Blot Analysis. Using RIPA buffer containing 1 mM PMSF and 1% phosphatase inhibitor cocktail, cell lysates were isolated. Using antibodies specific for PARP (T40050, Abmart, China), TrkB (WL00839, Wanleibio, China), GAPDH (M20006, Abmart, China), BCL-2 (T40056, Abmart, China), ERK1/2 (WL01864, Wanleibio, China) and p-ERK1/2 (Thr202/Tyr204) (WLP1512, Wanleibio, China), 20 μ g of protein was subjected to separation using SDS-PAGE and subsequently transferred onto PVDF membranes (BM3MB4254A, Millipore) for Western blot analysis. The HRP-labeled secondary antibody (A0208, Beyotime, China) was used to recognize the primary antibody, and ECL (P0018S, Beyotime, China) was employed to detect the antibody–antigen complex. The loading control for all blots was GAPDH. Band quantification was performed using ImageJ software.

RESULTS AND DISCUSSION

CADD Analysis. We conducted multiple rounds of virtual screening on 47,696 monomeric compounds of Chinese herbal medicine from 6,220 kinds of Chinese herbal medicine in the YaTCM database. The TCM natural product database YaTCM was used to mine compounds. The YaTCM database collected 47,696 natural products of Chinese medicine from 6220 kinds of Chinese herbal medicine as the ligand library for this study. The LigPrep module of Maestro 13.5 was used to perform

Table 1. continued

S.no	Compound	MF	mol MW	Smiles	Structural Formula
C11	6-Prenyleriodictyol	C ₂₀ H ₂₀ O ₆	372.50	<chem>CC(=CCC1=C(C2=C(C=C1)O)OC(CC2=O)C3=C(C=C(C=C3)O)O)O)C</chem>	
C12	(5R)-5-hydroxy-7-(4-hydroxy-3-methoxyphenyl)-1-phenylheptan-3-one	C ₂₀ H ₂₄ O ₄	358.52	<chem>COC1=C(C=CC(=C1)C[C@H](CC(=O)CCC2=CC=CC=C2)O)O</chem>	
C13	5-O-Methylhirsutanonol	C ₂₀ H ₂₄ O ₆	374.52	<chem>CO[C@@H](CCC1=C(C=C(C1)O)O)CC(=O)CCC2=CC(=C(C=C2)O)O</chem>	
C14	5-O-Ethylhirsutanonol	C ₂₁ H ₂₆ O ₆	388.54	<chem>CCO[C@@H](CCC1=C(C=C(C1)O)O)CC(=O)CCC2=CC(=C(C=C2)O)O</chem>	
C15	3-[2-(1,3-benzodioxol-5-yl)-7-methoxy-1-benzofuran-5-yl]propan-1-ol	C ₁₉ H ₁₈ O ₅	340.46	<chem>COC1=CC(=CC2=C1OC(=C2)C3=CC4=C(C=C3)OCO4)CCCO</chem>	
C16	7-(3,4-dihydroxy-5-methoxyphenyl)-5-hydroxy-1-(4-hydroxy-3-methoxyphenyl)heptan-3-one	C ₂₁ H ₂₆ O ₇	404.54	<chem>COC1=CC(=CC(=C1)O)O)CCC(CC(=O)CCC2=CC(=C(C=C2)O)OC)O</chem>	
C17	3"-Demethylhexahydro curcumin	C ₂₀ H ₂₄ O ₆	374.52	<chem>COC1=C(C=CC(=C1)C(CC(=O)C[C@H](CCC2=CC(=C(C=C2)O)O)O)O</chem>	
C18	5-hydroxy-7-(4-hydroxy-3-methoxyphenyl)-1-phenylheptan-3-one (DHPA)	C ₂₀ H ₂₄ O ₄	342.52	<chem>COC1=C(C=CC(=C1)C(CC(=O)CCC2=CC=CC=C2)O)O</chem>	
C19	7-(4-Hydroxy-3-methoxyphenyl)-5-methoxy-1-phenylheptan-3-one	C ₂₀ H ₂₄ O ₄	356.55	<chem>COC1=C(C=CC(=C1)C(CC(=O)CCC2=CC=CC=C2)OC)O</chem>	
C20	7-(4-hydroxyphenyl)-5-methoxy-1-phenylheptan-3-one	C ₂₀ H ₂₄ O ₃	326.52	<chem>COC(CCC1=CC=C(C=C1)O)CC(=O)CCC2=CC=CC=C2</chem>	

protonation, desalination, hydrogenation, generation of tautomers, generation of stereoconformations and energy minimization pretreatment of the molecules in the database. After pretreatment, due to tautomers, 58,048 prescreened compounds were obtained as the ligand library. Based on the drug accessibility rules "Lipinski Ro5" and "Verber Ro3" of the QickProp module of Maestro 13.5, the first round of screening was conducted, and 22,227 qualified hit compounds were

screened out. High-throughput virtual screening was conducted on the above hit compounds, and 2,955 hit compounds with the top 10% score were extracted based on the Glide module of Maestro 13.5. Standard precision screening was conducted, and the screened compounds were sorted again according to the Glide score, and 591 compounds with the top 10% were extracted. Ultraprecision screening was conducted, and 118 hit compounds with the top 10% score were retained

based on the Glide Grid module of Maestro 13.5. We screened out the top 20 hit compounds with the highest flexible docking score (Table 1), and performed toxicity prediction. As shown in Table 2, C1, C8, C9, C14, and C15 may have

Table 2. Predicted Values of Toxicity Parameters of Top 20 Hits and Positive Control

S.no	hepatotoxicity	nephrotoxicity	ames mutagenesis	acute oral toxicity
GW2580	−(51.25%)	−(56.96%)	+(57.00%)	III(73.65%)
C1	+(54.00%)	−(79.25%)	−(55.00%)	III(63.26%)
C2	−(50.72%)	+(45.53%)	−(73.00%)	III(69.60%)
C3	−(58.89%)	−(61.04%)	−(87.00%)	III(73.18%)
C4	−(60.72%)	+(69.16%)	−(50.00%)	III(65.13%)
C5	−(81.25%)	−(74.22%)	−(53.00%)	III(79.48%)
C6	−(53.72%)	−(64.57%)	−(58.00%)	III(59.86%)
C7	−(60.10%)	−(59.31%)	−(53.00%)	III(81.54%)
C8	+(52.70%)	−(68.06%)	−(58.00%)	III(79.30%)
C9	+(57.13%)	−(75.32%)	+(52.00%)	III(64.72%)
C10	−(51.25%)	+(46.98%)	+(55.00%)	III(53.35%)
C11	−(54.27%)	+(53.69%)	+(52.00%)	III(47.04%)
C12	−(59.13%)	−(78.62%)	−(74.00%)	III(67.11%)
C13	−(53.72%)	−(64.57%)	−(58.00%)	III(59.86%)
C14	+(51.28%)	+(47.72%)	−(57.00%)	III(73.62%)
C15	+(51.73%)	+(65.31%)	−(57.70%)	III(75.17%)
C16	−(50.38%)	−(63.50%)	−(75.00%)	III(69.20%)
C17	−(58.89%)	−(57.30%)	−(75.00%)	III(69.57%)
C18	−(60.38%)	−(75.24%)	−(74.00%)	III(67.11%)
C19	−(58.95%)	−(77.26%)	−(73.00%)	III(61.30%)
C20	−(61.45%)	−(90.70%)	−(74.00%)	III(67.11%)

hepatotoxicity; C2, C4, C10, C11, C14, and C15 may have nephrotoxicity; the positive control GW2580 and C9, C10, and C11 may undergo Ames mutagenesis. Except for the above compounds, C3, C5, C6, C7, C12, C13, C16, C17, C18, C19, and C20 have relatively ideal pharmacokinetic parameters and low predicted toxicity. Based on these results, MD simulations were used to further verify these 11 hit molecules, namely, C3, C5, C6, C7, C12, C13, C16, C17, C18, C19, C20.

Analysis of Binding Modes of Hit Compounds. In this study, GW2580 was used as a reference ligand to design and screen new inhibitors of TrkB. TrkB has the common main structural characteristics of protein kinases, including the N-lobe mainly in the form of β -strands, the C-lobe in the form of α -helices, and the hinge linker composed of residues 634 to 640 connecting the two lobes of the kinase. As shown in Figure 1, in the presence of GW2580, TrkB presents a clear DFG-out conformation.³⁰ In the DFG-out conformation, the phenylalanine (F) side chain in DFG occupies the ATP binding pocket, and the area formed by this conformation is not suitable for ATP binding and cannot accommodate the Mg^{2+} ions required for catalysis, and the side chain of aspartic acid (D) faces outside the active site. These changes make it difficult for ATP to bind to the kinase, thereby inhibiting the kinase activity. The central dimethoxy-benzyl part of GW2580 is stacked between the side chains of Val617 and Phe711 (DFG), and forms a π -stacking interaction with Phe633, and both oxygen atoms are within the interaction distance of the main chain amine of Asp710 (DFG); while the distal methoxyphenyl part is located in the hydrophobic pocket, the diamino-pyrimidine part of the ligand forms hydrogen bonds with the main chain carbonyls of the hinge residues

Glu634 and Met636, and is stacked between Ala586 and Leu699.³⁰ The design idea of this type II inhibitor not only binds to the ATP binding site in the kinase, but also extends the interaction to the allosteric site. Because its allosteric site is nonconservative, its selectivity is higher than that of traditional type I inhibitors.¹³

Interestingly, the top 11 hit compounds have some common structural characteristics: their cores consist of alkanes such as heptane, and most of the two ends are benzene rings, and most of the benzene rings have substituents such as phenolic hydroxyl groups. These hit compounds with heterocyclic or aromatic heterocyclic structures can form one or two hydrogen bonds with the hinge region, and their extended structures can occupy the exposed allosteric sites.

As shown in Figure 1, C3 forms hydrogen bond interactions with amino acids Arg696, Asn697 and Asp710 (DFG); C5 builds hydrogen bond interactions with Glu604 and Glu634 (hinge); C6 also forms hydrogen bond interactions with Glu604 and Glu634 (hinge); C7 forms hydrogen bond interactions with Asp710 (DFG) and Arg696; C12 builds hydrogen bond interactions with Val617 and Asp640 (hinge); C13 forms hydrogen bond interactions with Leu611 and Met636 (hinge); C16 forms hydrogen bond interactions with Lys588, Glu604 and Asp710 (DFG); C17 forms hydrogen bond interactions with Lys588 and Asp710 (DFG); C18 forms hydrogen bond interactions with Asp710 (DFG); C19 forms hydrogen bond interactions with Asp640 (hinge); C20 forms hydrogen bond interactions with Arg696. In addition, the benzene ring structure of the hit compounds can also form π - π interactions with the aromatic amino acids of the flexible N-terminal loop of Asp-Phe-Gly (DFG) of TrkB. Also as shown in Figure 1, C7, C19 and C20 all form π - π interactions with the amino acid Phe711 (DFG).

Pi-pi stacking is a weak interaction generated by the pi-electron conjugate system under specific spatial arrangements.³¹ Currently, the widely accepted forms of pi-stacking include pi-pi stacking, cation-pi stacking, anion-pi stacking, halogen bond-pi stacking, and CH-pi stacking.³² Such pi-stacking interactions play a key role in the recognition and binding process of protein-ligand interactions.³³ Therefore, pi-stacking is also widely used in the fields of drug design and molecular recognition. Many drug molecules achieve their therapeutic effects by binding to pi-stacking sites in biomolecules.³⁴ Many anticancer drugs and neurological drugs inhibit or activate the function of a specific protein target by generating π - π interactions with the aromatic amino acid residues of the target. Such effects often have good selectivity and affinity, thus becoming an important targeting strategy in drug design. However, although π - π interactions play an important role in the binding of drug molecules to biological targets, researchers still face many challenges, such as the precise quantification of this interaction and how to optimize this interaction to the greatest extent to improve the efficacy and selectivity of drug molecules. At the same time, it is also necessary to conduct in-depth research on how π - π interactions interact synergistically with other types of molecular interactions (such as hydrogen bonds and hydrophobic interactions) to fully understand the complex binding patterns between drug molecules and targets.

MD Simulation Analysis. MM/PBSA is an effective method for calculating the binding free energy of different complex systems. We used gmx_MMPBSA1.6.1 to calculate the binding free energy of 3000 conformations within the 30–

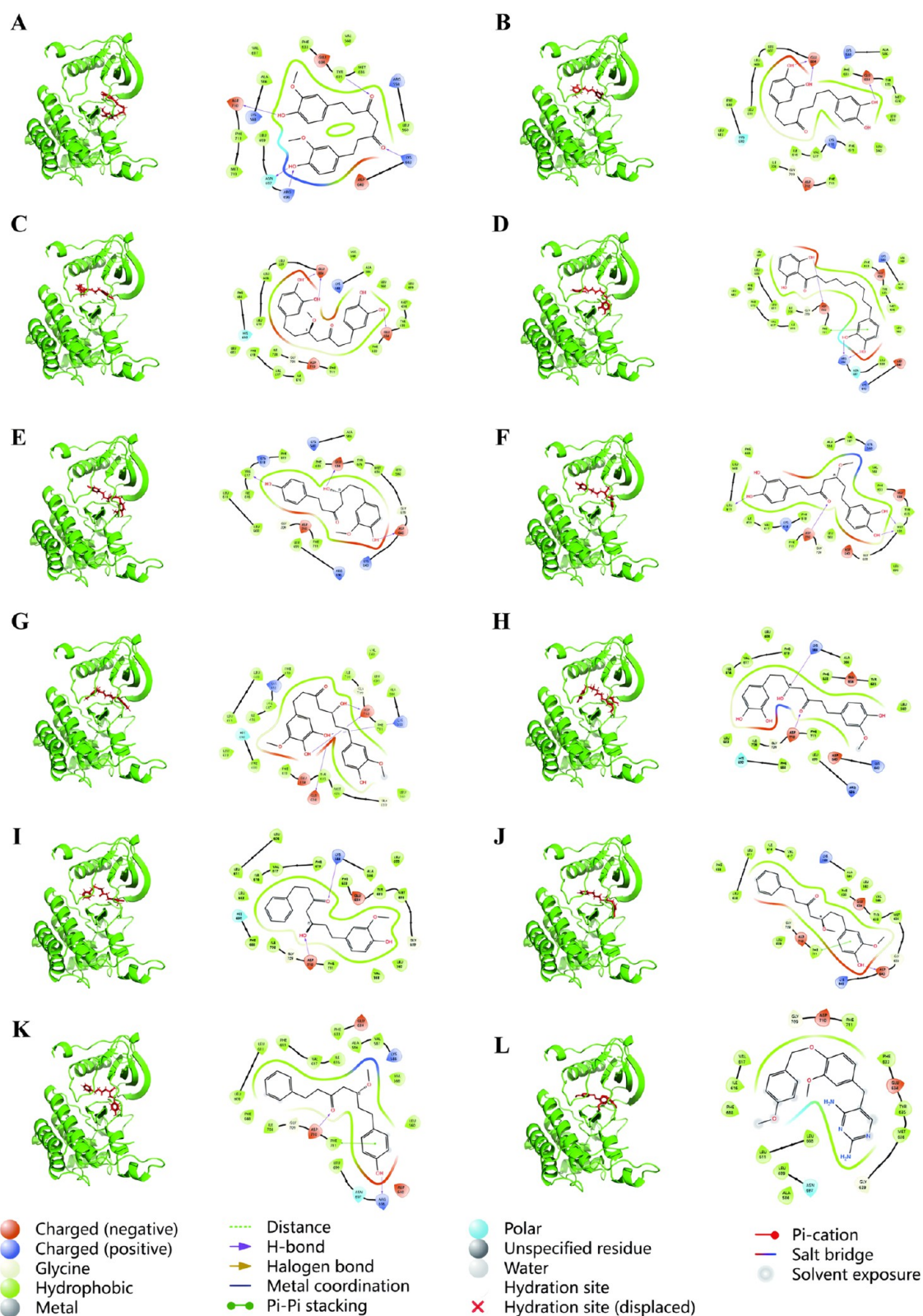


Figure 1. 3D/2D combination mode of flexible molecular docking between the hit compounds and TrkB. (A) TrkB-C3; (B) TrkB-C5; (C) TrkB-C6; (D) TrkB-C7; (E) TrkB-C12; (F) TrkB-C13; (G) TrkB-C16; (H) TrkB-C17; (I) TrkB-C18; (J) TrkB-C19; (K) TrkB-C20; (L) TrkB-GW2580.

60 ns simulation trajectory. As shown in Table 3, when C3, C7, and C13 combine with TrkB, the resulting ΔE_{vdW} is positive. ΔE_{vdW} refers to the van der Waals interaction force between molecules, which originates from the electrostatic interaction

between two molecules or atoms. When two atoms approach each other, their electron clouds overlap, thereby generating a strong repulsive force, which is inversely proportional to the 12th power of the distance. A positive ΔE_{vdW} value indicates

Table 3. MM/PBSA Binding Free Energy of Hits and Positive Control with Target TrkB (kcal/mol)

complex	ΔE_{vdW}	ΔE_{ele}	ΔG_{gas}	ΔG_{solv}	ΔG_{bind}
TrkB-C3	80.74 ± 257.20	-24.26 ± 10.27	56.48 ± 248.98	32.79 ± 8.90	89.27 ± 256.01
TrkB-C5	-43.10 ± 2.88	-35.66 ± 12.52	-78.75 ± 11.32	34.84 ± 4.98	-43.91 ± 6.84
TrkB-C6	-45.09 ± 4.19	-45.30 ± 12.63	-90.40 ± 8.82	43.60 ± 7.50	-46.80 ± 3.98
TrkB-C7	46.24 ± 199.31	-26.35 ± 9.75	19.89 ± 205.34	30.01 ± 4.72	49.90 ± 201.95
TrkB-C12	-46.69 ± 4.25	-23.36 ± 5.73	-69.85 ± 8.89	30.51 ± 3.87	-39.34 ± 6.18
TrkB-C13	45.81 ± 191.79	-28.46 ± 7.34	17.35 ± 194.14	34.46 ± 5.37	51.81 ± 197.35
TrkB-C16	-52.36 ± 4.82	-28.27 ± 12.16	-80.64 ± 9.77	34.70 ± 6.15	-45.94 ± 5.40
TrkB-C17	-50.18 ± 2.78	-24.50 ± 8.82	-74.49 ± 8.58	33.33 ± 5.84	-41.16 ± 4.35
TrkB-C18	-47.34 ± 2.10	-20.09 ± 4.40	-67.42 ± 4.71	26.10 ± 3.39	-41.32 ± 2.35
TrkB-C19	-47.22 ± 4.32	-14.39 ± 5.71	-61.62 ± 7.74	21.49 ± 4.09	-40.12 ± 5.17
TrkB-C20	-47.63 ± 2.43	-19.75 ± 6.02	-67.37 ± 6.21	26.74 ± 4.56	-40.63 ± 3.04
TrkB-GW2580	-56.04 ± 1.40	-21.96 ± 2.24	-78.00 ± 2.50	27.13 ± 1.65	-50.88 ± 2.13

that the van der Waals interaction energy between the protein and the ligand shows an upward trend. This means that the van der Waals attraction between the two is gradually weakening, which suggests that at the level of van der Waals interaction, the binding of the protein and the ligand is in a relatively unfavorable situation. The calculation results of ΔG_{bind} for the above three systems are also positive, which means that the binding process of the protein and the ligand is thermodynamically unfavorable. A positive binding free energy usually indicates that the binding process does not occur spontaneously and requires external energy supply to achieve binding. Further speaking, this implies that the binding of C3, C7, and C13 with TrkB is energetically unstable. Compared to the case where the binding free energy is negative, the positive result suggests that this binding is relatively fragile and is prone to dissociation due to interference from external factors. Among the TrkB-C5, TrkB-C6, TrkB-C12, TrkB-C16, TrkB-C17, TrkB-C18, TrkB-C19, TrkB-C20, and TrkB-GW2580 systems, the binding energy is relatively strong, and the ΔG_{bind} of these systems is all below -30 kcal/mol.

To explore the dynamic characteristics of the interaction between small molecule inhibitors and TrkB, we conducted 60 ns MD simulations using five crystal structures of TrkB as the initial structures, and each complex simulation was repeated 3 times. Next, we calculated the RMSD value to measure whether the binding of the protein–ligand complex is robust. Figures 2 and 3 show the RMSD fluctuations of the protein–ligand complex throughout the simulation process. During the entire simulation process, the RMSD values of TrkB–C6, TrkB–C12, TrkB–C17, TrkB–C18, and TrkB–C19 fluctuated slightly and converged to an equilibrium state within the simulated time range. However, for systems such as 4AT1–1 in TrkB–C5, 4AT3–3 and 4AT4–3 in TrkB–C6, 4AT4–1 and 4F0I–1 in TrkB–C16, and 4AT4–3 in TrkB–C20, there were still significant fluctuations after 50 ns of the simulation and did not reach a convergent equilibrium state. Based on the above RMSD results, in the 60 ns MD simulation, the binding of the protein–ligand complexes TrkB–C6, TrkB–C12, TrkB–C17, TrkB–C18, and TrkB–C19 is robust.

The key regions for the design of TrkB inhibitors include the hinge region (Glu634, Tyr635, Met636, Lys637, His638, Gly639, Asp640) and the DFG region (Asp710, Phe711, Gly712). To conduct in-depth analysis and screen out compounds that have a significant impact on the key residues in the hinge region and the DFG region, we start from studying the influence of hit compounds on the fluctuation of these key amino acid residues. As shown in Table 4, when GW2580 is

present, compared with the simulation of TrkB protein alone, the RMSF values of amino acid residues in the above key regions are all reduced. This result indicates that GW2580 can weaken the fluctuation of amino acid residues in these regions, and this phenomenon can be attributed to the interaction between GW2580 and this region. By accurately calculating the RMSF, we found that among C6, C12, C17, C18, and C19, only C17 and C18 have an impact on the key amino acid residues of TrkB similar to that of the positive control GW2580. Thus, it can be inferred that C17 and C18 are more likely to become TrkB inhibitors similar to GW2580.

By observing the energy valleys in the free energy landscape diagram, the stability of the binding between the protein and the ligand can be determined. Deeper and more single energy valleys usually indicate more stable binding. Based on this, in this study, the mean values of RMSD and Rg from 15 simulations of each system were used as two important variables to describe the characteristics of the TrkB–ligand complex system, and the free energy landscape diagrams of TrkB–C17, TrkB–C18 and TrkB–GW2580 were drawn. As shown in Figure 4, the TrkB–C17, TrkB–C18, and TrkB–GW2580 complexes all formed a single energy valley, indicating that their binding with TrkB is stable. This is consistent with the results we obtained earlier through RMSD.

Based on the results of MM/PBSA, RMSD, and FEL mentioned above, it can be considered that the binding of C17 and C18 to TrkB are relatively stable, and the binding energy is good, which is worthy of further study and verification.

SMD Simulation and US Analysis. SMD and US are two computational methods used to explore the interaction between molecules. The SMD simulation is based on MD simulation. By applying a tensile external force to the molecules, the binding and dissociation processes between molecules can be observed. US is based on SMD simulation. Sampling is carried out at different tensile distances to obtain the free energy curves of binding and dissociation between molecules.

These two methods can be used to study the interaction among TrkB–C17, TrkB–C18 and TrkB–GW2580 as well as their binding and dissociation processes. Through the analysis of these processes, information such as binding and dissociation constants, and binding and dissociation free energies can be obtained, providing a strong basis for analyzing the binding situation of receptors and ligands. C17 (Figure 5A), C18 (Figure 5D), or GW2580 (Figure 5G) are all stretched along the positive X-axis from their binding positions with TrkB. The relationship between the tensile displacement

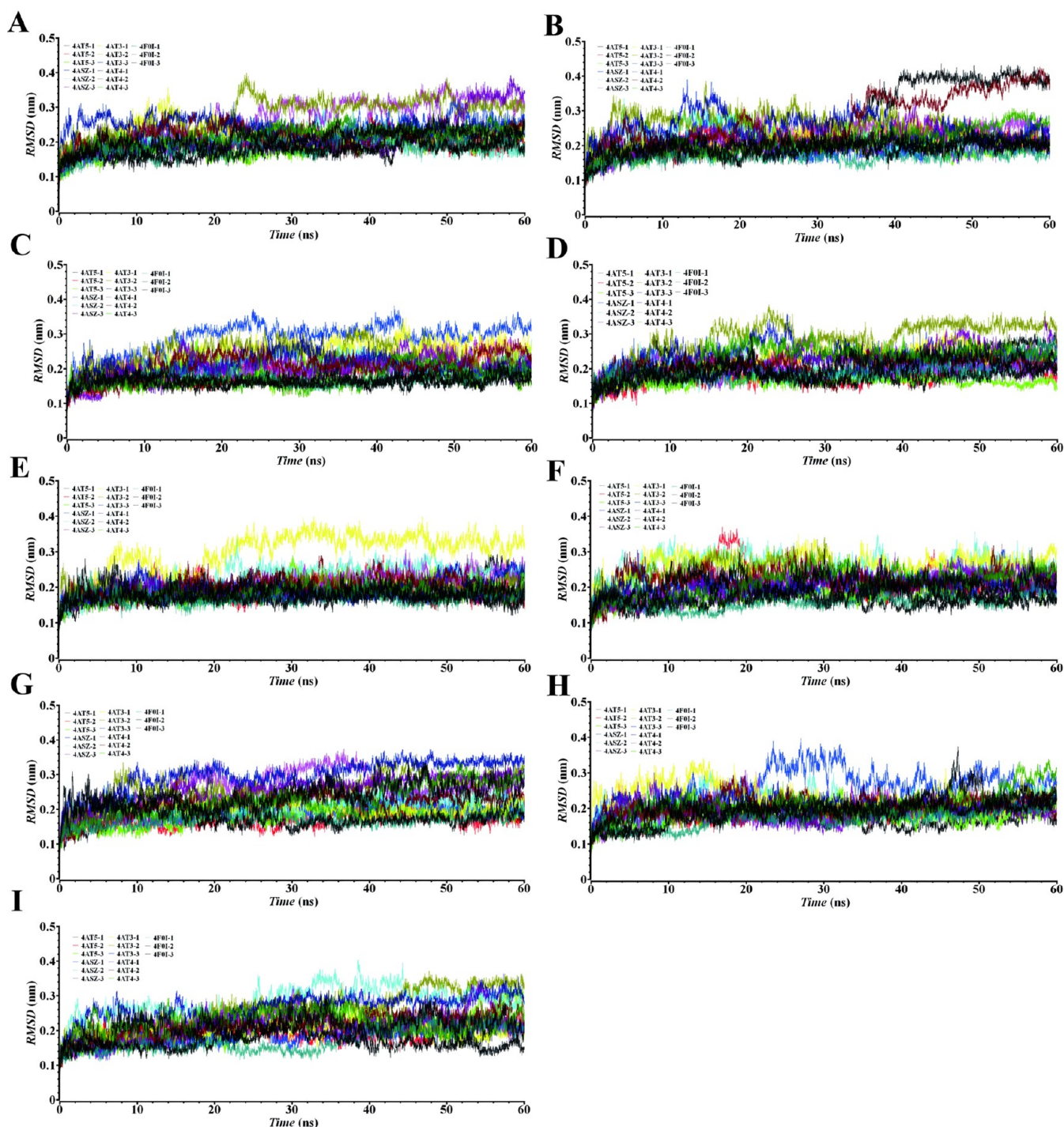


Figure 2. RMSD graph of TrkB protein backbone in all complexes during 60 ns MD simulation. (A):TrkB-C5; (B):TrkB-C6; (C):TrkB-C12; (D):TrkB-C16; (E):TrkB-C17; (F):TrkB-C18; (G):TrkB-C19; (H):TrkB-C20; (I):TrkB- GW2580.

of C17 and TrkB and the harmonic spring force is shown in Figure 5B, and the dissociation free energy curve of C17 is shown in Figure 5C. The relationship between the tensile displacement of C18 and TrkB and the harmonic spring force is shown in Figure 5E, and the dissociation free energy curve of C18 is shown in Figure 5F. The relationship between the tensile displacement of GW2580 and TrkB and the harmonic spring force is shown in Figure 5H, and the dissociation free energy curve of GW2580 is shown in Figure 5I. The ΔG of TrkB–C17 is approximately -38.37 kJ/mol, the ΔG of TrkB–C18 is approximately -41.62 kJ/mol, and the ΔG of TrkB–

GW2580 is approximately -46.63 kJ/mol. When using the US technique, we adopted the weighted histogram analysis method (WHAM) to quantitatively calculate the free energy change from the binding to the dissociation process of TrkB and the hit compounds from the perspective of statistical mechanics, and thereby obtain the dissociation energy. In this way, we can deeply understand the microscopic mechanical mechanisms involved in the binding and dissociation processes of proteins–ligands, providing a crucial theoretical foundation at the molecular level for studying the interaction between TrkB and hit compounds. This is also a revalidation of the

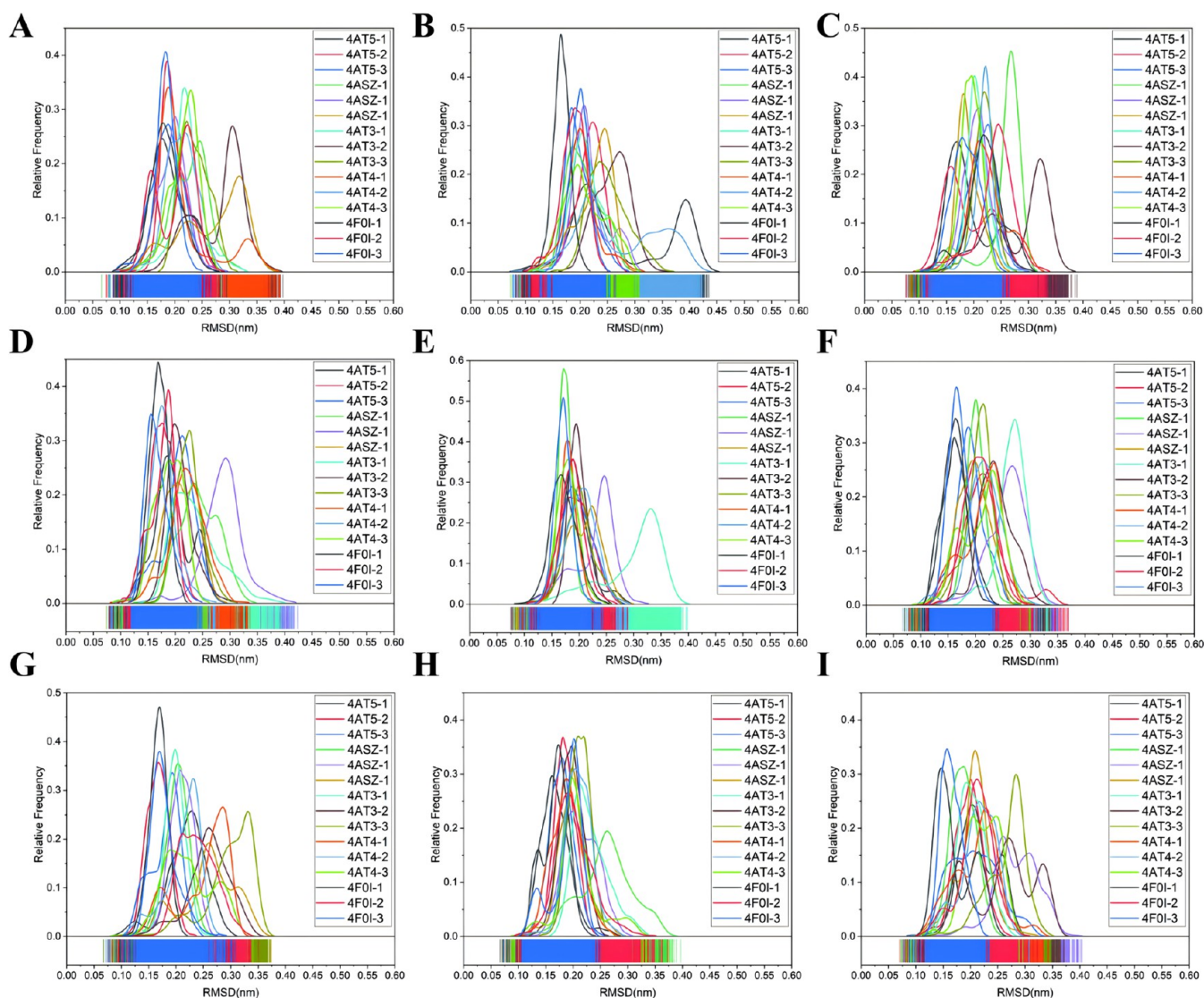


Figure 3. Normal distribution curves of the relative frequencies of RMSD values of the TrkB protein backbone in all complexes during 60 ns MD simulation. (A):TrkB-C5; (B):TrkB-C6; (C):TrkB-C12; (D):TrkB-C16; (E):TrkB-C17; (F):TrkB-C18; (G):TrkB-C19; (H):TrkB-C20; (I):TrkB- GW2580.

Table 4. RMSF Value of Residues in Key Structural Domains of the Complex of Hits and Positive Control with Target TrkB (Å)

key residue	TrkB	GW2580	C6	C12	C17	C18	C19
Glu634(Hinge)	0.66 ± 0.11	0.65 ± 0.05	0.64 ± 0.12	0.65 ± 0.10	0.67 ± 0.09	0.65 ± 0.09	0.69 ± 0.08
Tyr635(Hinge)	0.68 ± 0.10	0.70 ± 0.05	0.72 ± 0.14	0.71 ± 0.10	0.77 ± 0.13	0.72 ± 0.11	0.76 ± 0.11
Met636(Hinge)	0.67 ± 0.05	0.67 ± 0.05	0.71 ± 0.11	0.71 ± 0.10	0.70 ± 0.09	0.73 ± 0.09	0.77 ± 0.09
Lys637(Hinge)	0.73 ± 0.07	0.72 ± 0.05	0.78 ± 0.10	0.76 ± 0.09	0.76 ± 0.09	0.75 ± 0.09	0.82 ± 0.08
His638(Hinge)	0.72 ± 0.06	0.69 ± 0.06	0.76 ± 0.09	0.71 ± 0.09	0.71 ± 0.07	0.71 ± 0.08	0.75 ± 0.09
Gly639(Hinge)	0.66 ± 0.07	0.64 ± 0.06	0.70 ± 0.07	0.68 ± 0.09	0.67 ± 0.06	0.66 ± 0.06	0.70 ± 0.59
Asp640(Hinge)	0.55 ± 0.06	0.55 ± 0.06	0.58 ± 0.05	0.57 ± 0.09	0.55 ± 0.05	0.55 ± 0.05	0.59 ± 0.08
Asp710(DFG)	0.87 ± 0.31	0.65 ± 0.16	0.65 ± 0.18	0.76 ± 0.20	0.72 ± 0.16	0.66 ± 0.15	0.72 ± 0.21
Phe711(DFG)	1.01 ± 0.31	0.77 ± 0.19	0.83 ± 0.33	0.86 ± 0.20	0.91 ± 0.25	0.85 ± 0.30	0.69 ± 0.31
Gly712(DFG)	1.01 ± 0.23	0.96 ± 0.24	0.98 ± 0.38	0.98 ± 0.26	1.05 ± 0.24	0.99 ± 0.37	0.69 ± 0.41

results of MM/PBSA from the perspective of dissociation. It has been fully confirmed that C17 and C18 can stably bind to TrkB like the positive control GW2580. Nevertheless, the results of computational simulations still need to be verified by experimental means.

DHPA(C18) Can Inhibit the Growth and Survival of NB Cells. In this study, the expression of the NTRK2 gene in nine human NB cell lines from different sources was analyzed using the Cancer Cell Line Encyclopedia (CCLE) database (broadinstitute.org), and NTRK2 is the gene encoding TrkB. As shown in Figure 6A, among the NB cell lines, those with

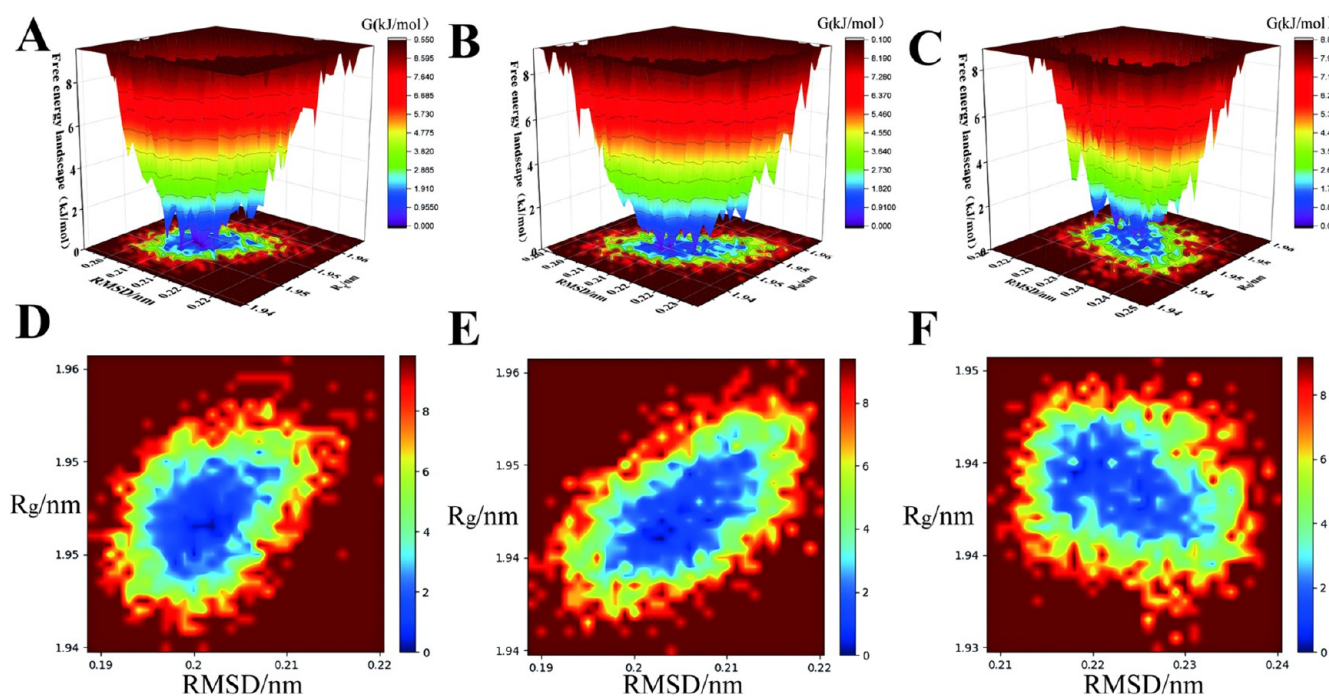


Figure 4. FEL of the complexes during 30–60 ns MD simulation. (A,D)TrkB-C17; (B,E):TrkB-C18; (C,F):TrkB-GW2580.

relatively high expression of NTRK2 were SK-N-SH, SK-N-BE(2), and KELLY. To explore the effects of 3''-demethylhexahydrocurcumin (C17) and DHPA (C18) on the proliferation of NB cell lines, different concentrations of 3''-demethylhexahydrocurcumin (C17) were added to SK-N-BE(2) and KELLY cells respectively, and different concentrations of DHPA (C18) were added to SK-N-SH, SK-N-BE(2), and KELLY cells, respectively. All were cultured for 48 h. The results of the CCK-8 experiment showed that the IC_{50} of 3''-demethylhexahydrocurcumin (C17) in SK-N-BE(2) cells is 39.32 $\mu\text{g/mL}$, and in KELLY cells is 39.25 $\mu\text{g/mL}$; the IC_{50} of DHPA (C18) in SK-N-SH cells is 1.686 $\mu\text{g/mL}$, in SK-N-BE(2) cells is 8.886 $\mu\text{g/mL}$, and in KELLY cells is 0.4969 $\mu\text{g/mL}$. Compared with C17 (Figure 6B,C), C18 (Figure 6D–F) can significantly inhibit cell growth. Microscopic examination results showed that 10 $\mu\text{g/mL}$ of DHPA (C18) can significantly inhibit the cell growth of the NB cell line SK-N-BE(2) (Figure 6G).

Furthermore, in the colony formation assay, compared with the control group, DHPA(C18) (10 $\mu\text{g/mL}$) significantly reduced the proliferation of NB (Figure 7A). The flow cytometry study of cell apoptosis showed that DHPA(C18) could block the proliferation of tumor cells and induce apoptosis (Figure 7B). The results of the cell cycle study showed that DHPA(C18) treatment led to a significant reduction in the number of G1 phase cells in NB cells, while the number of S phase cells increased (Figure 7C). The expression of PARP and BCL-2 in the DHPA(C18) group decreased significantly, which is an indicator of cell apoptosis (Figure 7D). Overall, these data indicate that the small molecule inhibitor DHPA (C18) of TrkB can kill NB cells and inhibit their proliferation.

DHPA(C18) May Be a Potential Inhibitor of TrkB. The effect of DHPA (C18) on the expression of target protein TrkB was detected by WB technology. As shown in Figure 8A,B, with the continuous increase of DHPA (C18) concentration, the expression level of TrkB decreased

significantly. This finding indicates that DHPA (C18) can down-regulate the expression of TrkB. At the same time, similar results were obtained from the immunofluorescence experiment. As shown in Figure 8D, TrkB is highly expressed on the cell membrane. Compared with the control group, the expression of TrkB on the cell membrane in the DHPA (C18) treatment group decreased significantly.

MAPK is the classic downstream signaling pathway of TrkB. The phosphorylation level of ERK is a key indicator for evaluating whether the MAPK signaling pathway is activated. As shown in Figure 8A,C, DHPA (C18) can significantly inhibit the phosphorylation of ERK. This result indicates that DHPA (C18) can inhibit the activation of the downstream signaling pathway of TrkB.

Cellular thermal shift assay (CETSA) is an experimental technique used to detect the binding efficiency of drugs to intracellular target proteins. The principle is that when a target protein binds to a drug molecule, it usually changes the thermal stability of the protein. In each temperature setting, the previous lane is set as DMSO, and the subsequent lane is DHPA (C18) dissolved in the same volume of DMSO. As can be seen from Figure 8E, compared with the control group, the thermal stability of TrkB protein in the DHPA (C18) group increased significantly at 50 $^{\circ}\text{C}$; while at 55, 60, and 65 $^{\circ}\text{C}$, the thermal stability of TrkB protein in the DHPA (C18) group decreased extremely significantly. The above preliminary results indicate that DHPA (C18) can affect the thermal stability of TrkB. This change may be due to the binding of DHPA (C18) to TrkB, resulting in a conformational change of TrkB.

The drug affinity responsive target stability (DRATS) experiment is an experimental technique that can effectively determine the binding ability of drugs to specific target proteins and evaluate the impact of drugs on the stability of target proteins. The main principle of this experiment is that when a small molecule drug binds to a target protein, it can significantly increase the digestion stability of the target protein

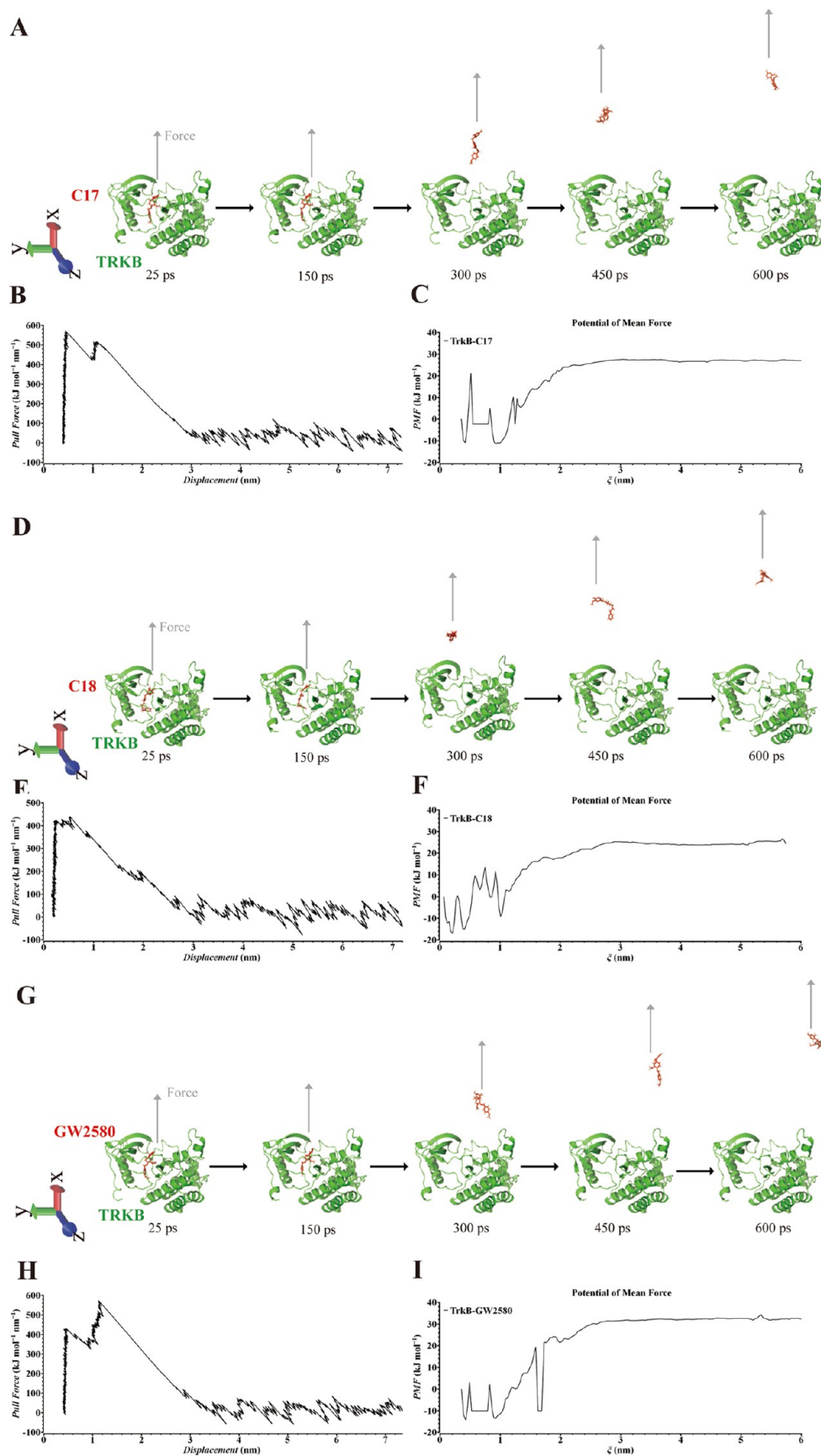


Figure 5. SMD and US simulations of TrkB-C17, TrkB-C18 and TrkB-GW2580. Schematic diagram of the SMD of TrkB-C17(A), TrkB-C18(D) and TrkB-GW2580(G). The relationship between the force on the harmonic spring and the displacement during the SMD separation process of TrkB-C17(B), TrkB-C18(E) and TrkB-GW2580(H). PMF values of TrkB-C17(C), TrkB-C18(F) and TrkB-GW2580(I) calculated by the WHAM algorithm.

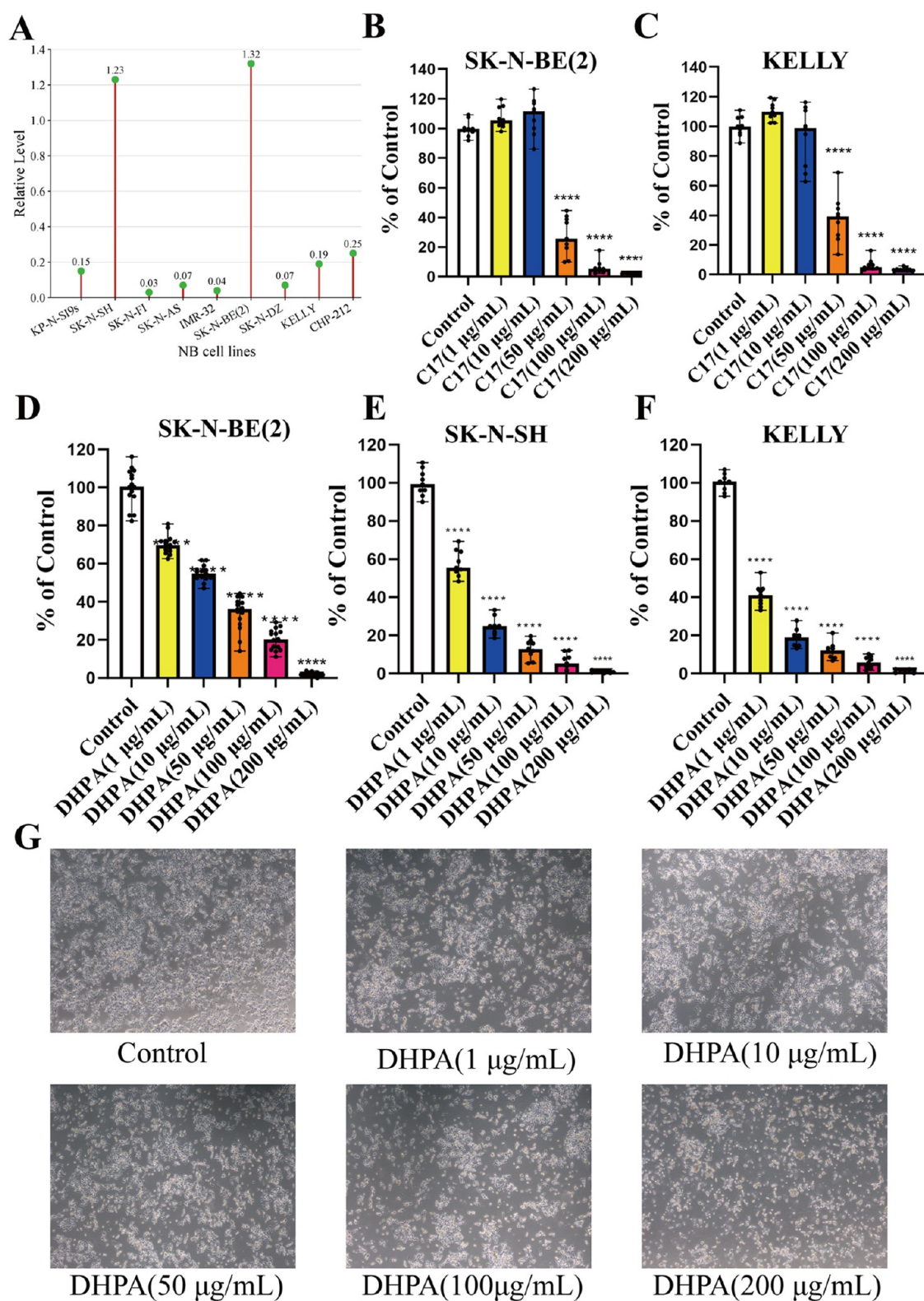


Figure 6. (A) Analysis of NTRK2 gene expression in nine human NB cell lines via CCLE database. (B) The CCK-8 assay reveals the difference in cell viability between control and treated with 3'-Demethylhexahydrocurcumin (C17) in SK-N-BE(2). (C) The CCK-8 assay reveals the difference in cell viability between control and treated with 3'-Demethylhexahydrocurcumin (C17) in KELLY. (D) The CCK-8 assay reveals the difference in cell viability between control and treated with DHPA (C18) in SK-N-BE(2). (E) The CCK-8 assay reveals the difference in cell viability between control and treated with DHPA (C18) in SK-N-SH. (F) The CCK-8 assay reveals the difference in cell viability between control and treated with DHPA (C18) in KELLY. (G) Representative images of SK-N-BE(2) cells treated with control or DHPA. **** $P < 0.0001$, two groups' statistical differences were contrasted using the student's t test. Data were representative of at least three independent experiments.

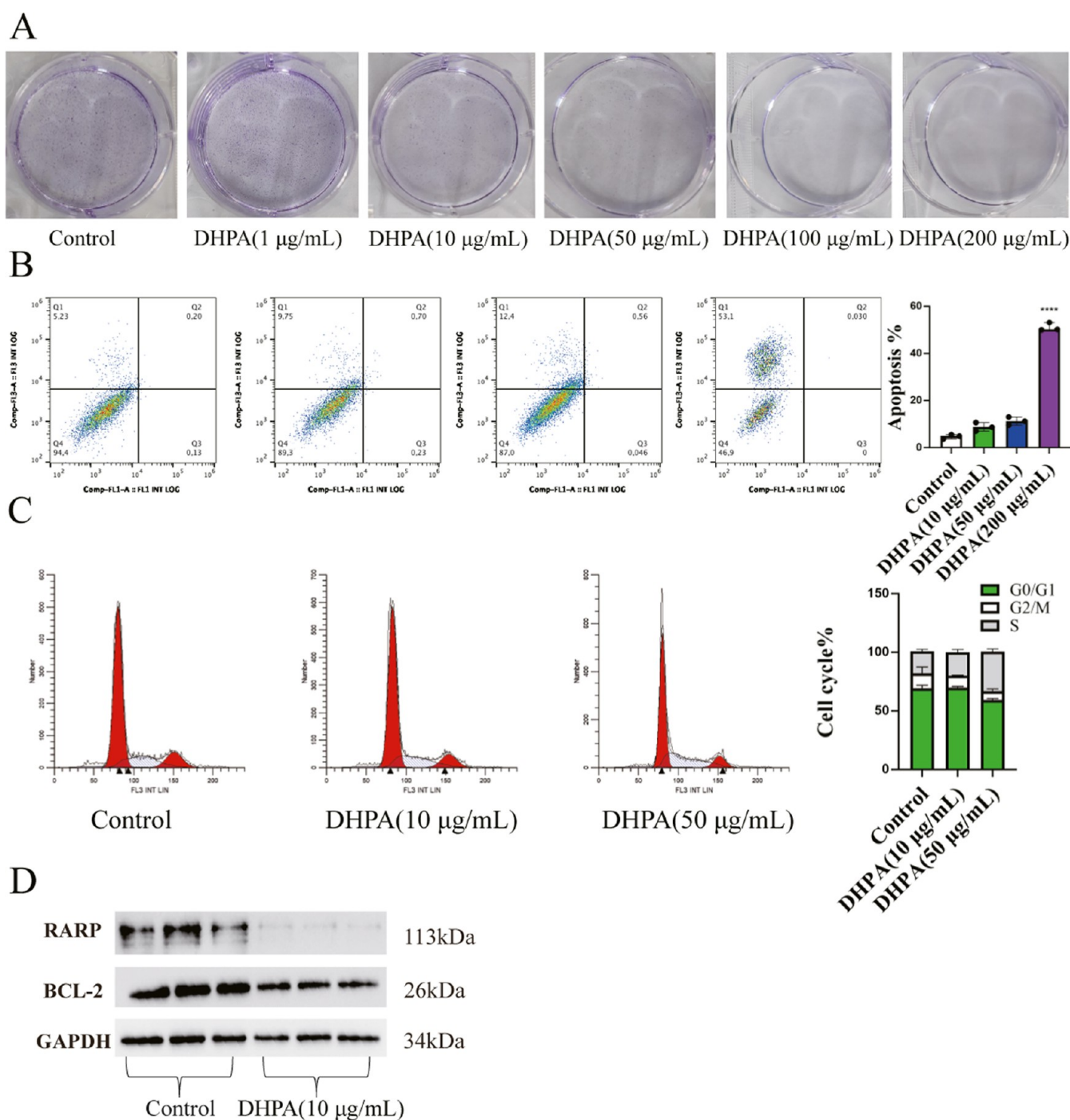


Figure 7. (A) Colony formation assay images and quantification depicting the growth of NB cells between control and treated with DHPA. (B) Flow cytometry analysis demonstrating the apoptosis of NB cells between control and treated with DHPA. Apoptotic index is defined as the ratio between Q2 and Q3 over total cells. (C) Flow cytometry depicting cell cycle distribution of SK-N-BE(2) cells between control and treated with DHPA. (D) Western blot revealing apoptosis related markers in NB cells between control and treated with DHPA (10 µg/mL).

to proteases. As shown in Figure 8F, compared with the DMSO control group, the DHPA treatment group showed higher stability against the degradation of streptomycin protease, and its degradation degree was significantly lower than that of the DMSO group. It can be inferred that this resistance to the degradation of streptomycin protease may be caused by the binding of DHPA to TrkB. The above experiments indirectly indicate that DHPA (C18) may bind to TrkB.

CONCLUSIONS

Among children, NB is a rare but highly malignant solid tumor. Given the heterogeneity of this disease, current treatment methods often fail to be effective. Since NB poses a serious threat to children's health and has a high mortality rate, exploring new treatment strategies is extremely urgent. The current research focus is mainly on determining the commonalities among different types of NB and actively developing new strategies such as targeted therapy to improve treatment outcomes. In our study, the TrkB model was

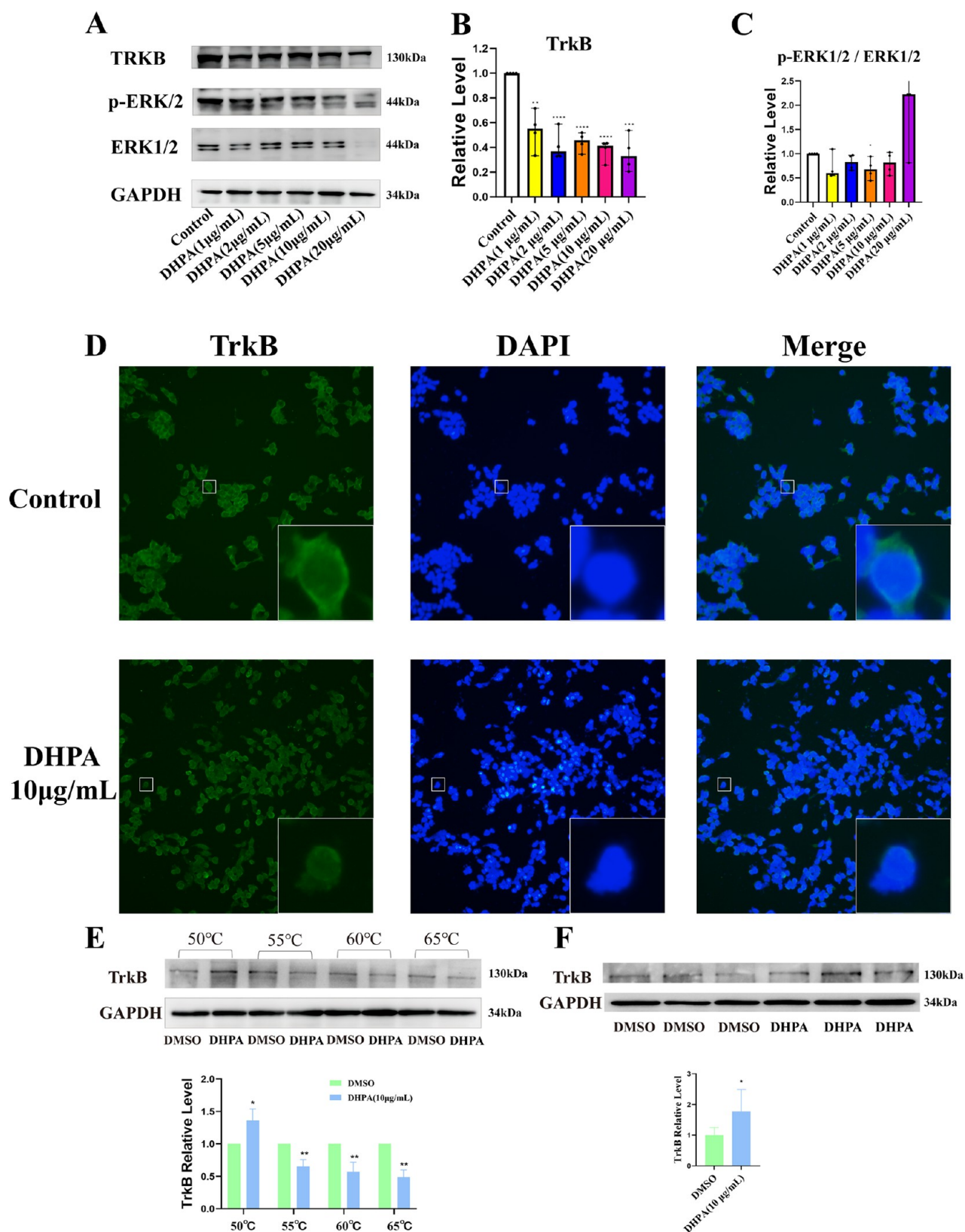


Figure 8. (A) Western blot showing the expression of TrkB, ERK1/2 and p-ERK1/2 between the control group and the group treated with DHPA. (B) The relative expression of TrkB between the control group and the group treated with DHPA. (C) The relative expression of p-ERK1/2 and ERK1/2 between the control group and the group treated with DHPA. (D) The immunofluorescence results of TrkB between the control group and the group treated with DHPA. (E) The CETSA results of TrkB between the DMSO group and the group treated with DHPA(10 μ g/mL). (F) The DARTS results of TrkB between the DMSO group and the group treated with DHPA(10 μ g/mL). * $P < 0.05$, ** $P < 0.01$, *** $P < 0.001$, **** $P < 0.0001$, two groups' statistical differences were contrasted using the student's t test. Data were representative of at least 3 independent experiments.

constructed with the protein database structure 4AT5. Under the guidance of the ligand-based electronic pharmacophore in the YaTCM, virtual screening was conducted on TCM natural product compounds to search for those that might bind to TrkB. MD simulations were used to virtually verify the binding ability of the screened compounds to TrkB. On this basis, SMD simulations and US simulations were used to innovatively reverify the binding ability of the screened compounds to TrkB. Among the top 11 optimized hit compounds, DHPA and 3''-demethylhexahydrocurcumin stood out. Further simulations showed that they formed stable receptor–ligand binary complexes with TrkB. In subsequent *in vitro* cell experiments, 3''-demethylhexahydrocurcumin was eliminated because of its high IC₅₀ for killing NB cells. A relatively low concentration of DHPA can significantly kill NB cells. Moreover, DHPA can inhibit the expression of TrkB, the activation of the downstream signaling pathway of TrkB, and affect the thermal stability of TrkB protein and the response to the degradation effect of streptomycin protease. The above results indicate that DHPA may be a potential TrkB inhibitor. The method we used, which combines electronic pharmacophores, structure-based virtual screening, and MD simulations, highlights the effectiveness of computational methods in accelerating the drug discovery process. However, future studies should fully consider the potential benefits and possible side effects of DHPA, and further verification through *in vivo* experiments is needed to determine its reliability and therapeutic efficacy in the treatment of NB.

■ ASSOCIATED CONTENT

Data Availability Statement

The information about CADD and MD simulation is available on GitHub at <https://github.com/bookasiap/li-zhong>. We uploaded the representative files but the full length files are too big to upload on GitHub, so the trajectory files are available upon request to the corresponding author (Zhong Li).

■ AUTHOR INFORMATION

Corresponding Author

Zhong Li – Department of Pharmacy, Dalian Women and Children's Medical Group, Dalian, Liaoning 116012, China; orcid.org/0000-0002-5957-8486; Email: lzong163@163.com

Authors

Tianyi Liu – Department of Pharmacy, Dalian Women and Children's Medical Group, Dalian, Liaoning 116012, China
Hongli Yin – Institute of Pediatric Research, Children's Hospital of Soochow University, Suzhou 215025, China
Qingyang Hu – College of Pharmacy, Dalian Medical University, Dalian, Liaoning 116044, China
Xue Dong – College of Pharmacy, Dalian Medical University, Dalian, Liaoning 116044, China
Bin Xin – College of Pharmacy, Dalian Medical University, Dalian, Liaoning 116044, China
Yue Wu – College of Pharmacy, Dalian Medical University, Dalian, Liaoning 116044, China
Xuejiao Hu – College of Pharmacy, Dalian Medical University, Dalian, Liaoning 116044, China
Wenxin Yan – College of Pharmacy, Dalian Medical University, Dalian, Liaoning 116044, China

Complete contact information is available at:

<https://pubs.acs.org/10.1021/acsomega.4c04528>

Author Contributions

||T.L., H.Y. and Q.H. contributed equally to this work. T.L.: writing—original draft, methodology, software. H.Y.: validation, data curation. Q.H.: resources, visualization, formal analysis. X.D.: formal analysis. B.X.: investigation. Y.W.: visualization. X.H.: visualization. W.Y.: investigation. Z.L.: project administration, writing—review and editing.

Funding

This work was supported by Dalian Science and Technology Innovation Fund (2023JJ13SN044) to Z.L.; Natural Science Foundation of Jiangsu Province (BK20230217) to H.Y.; Science and Technology Program of Suzhou (SKY2023193) to H.Y.

Notes

The authors declare no competing financial interest.

■ ACKNOWLEDGMENTS

The authors are thankful to the Key Laboratory for Early Diagnosis and Biotherapy of Malignant Tumors in Children and Women, Dalian Women and Children's Medical Group, Dalian, Liaoning Province, China, for providing necessary facilities to carry out this research work.

■ ABBREVIATIONS

NB:neuroblastoma; NTRK:neurotrophic receptor tyrosine kinase; TrkB:tropomyosin receptor kinase B; TCM:traditional Chinese medicine; CADD:computer-aided drug design; MD:molecular dynamics; SMD:stretching molecular dynamics; US:umbrella sampling; DHPA:5-hydroxy-7-(4-hydroxy-3-methoxyphenyl)-1-phenylheptan-3-one; PDB:Protein Data Bank; YaTCM:natural product database of TCM; HTVS:high-throughput virtual screening; SP:standard precision; XP:extra precision; NVT:number of particles, volume; NPT:temperature; number of particles, pressure, temperature; MM/PBSA:molecular mechanics Poisson–Boltzmann surface area; RMSD:root-mean-square deviation; RMSF:root-mean-square fluctuation; FEL:free energy landscape

■ REFERENCES

- (1) Skertich, N. J.; Chu, F.; Tarhoni, I. A. M.; Szajek, S.; Borgia, J. A.; Madonna, M. B. Expression of Immunomodulatory Checkpoint Molecules in Drug-Resistant Neuroblastoma: An Exploratory Study. *Cancers* **2022**, *14* (3), No. 751, DOI: 10.3390/cancers14030751.
- (2) Qiu, B.; Matthey, K. K. Advancing therapy for neuroblastoma. *Nat. Rev. Clin. Oncol.* **2022**, *19* (8), 515–533.
- (3) Aygun, N. Biological and Genetic Features of Neuroblastoma and Their Clinical Importance. *Curr. Pediatr. Rev.* **2018**, *14* (2), 73–90.
- (4) Hou, R.; Yu, Y.; Jiang, J. Prostaglandin E2 in neuroblastoma: Targeting synthesis or signaling? *Biomed. Pharmacother.* **2022**, *156*, No. 113966.
- (5) Zafar, A.; Wang, W.; Liu, G.; Wang, X.; Xian, W.; McKeon, F.; Foster, J.; Zhou, J.; Zhang, R. Molecular targeting therapies for neuroblastoma: Progress and challenges. *Med. Res. Rev.* **2021**, *41* (2), 961–1021.
- (6) Larotrectinib. *Drugs and Lactation Database (LactMed)*; National Institute of Child Health and Human Development: Bethesda (MD), 2006.
- (7) Entrectinib. *LiverTox: Clinical and Research Information on Drug-Induced Liver Injury*; National Institute of Diabetes and Digestive and Kidney Diseases: Bethesda (MD), 2012.

- (8) Basri, A. M.; Taha, H.; Ahmad, N. A Review on the Pharmacological Activities and Phytochemicals of *Alpinia officinarum* (Galangal) Extracts Derived from Bioassay-Guided Fractionation and Isolation. *Pharmacogn. Rev.* **2017**, *11* (21), 43–56.
- (9) Rani, Y. G.; Lakshmi, B. S. Structural insight into the antagonistic action of diarylheptanoid on human estrogen receptor alpha. *J. Biomol. Struct. Dyn.* **2019**, *37* (5), 1189–1203.
- (10) Honmore, V. S.; Kandhare, A. D.; Kadam, P. P.; Khedkar, V. M.; Sarkar, D.; Bodhankar, S. L.; Zangwar, A. A.; Rojatkar, S. R.; Natu, A. D. Isolates of *Alpinia officinarum* Hance as COX-2 inhibitors: Evidence from anti-inflammatory, antioxidant and molecular docking studies. *Int. Immunopharmacol.* **2016**, *33*, 8–17.
- (11) Shin, J. E.; Han, M. J.; Song, M. C.; Baek, N. I.; Kim, D. H. 5-Hydroxy-7-(4'-hydroxy-3'-methoxyphenyl)-1-phenyl-3-heptanone: a pancreatic lipase inhibitor isolated from *Alpinia officinarum*. *Biol. Pharm. Bull.* **2004**, *27* (1), 138–140.
- (12) Cai, Y.; Xiao, R.; Zhang, Y.; Xu, D.; Wang, N.; Han, M.; Zhang, Y.; Zhang, L.; Zhou, W. DHPA Protects SH-SY5Y Cells from Oxidative Stress-Induced Apoptosis via Mitochondria Apoptosis and the Keap1/Nrf2/HO-1 Signaling Pathway. *Antioxidants* **2022**, *11* (9), No. 1794, DOI: 10.3390/antiox11091794.
- (13) Berstrand, T.; Kothe, M.; Liu, J.; Dupuy, A.; Rak, A.; Berne, P. F.; Davis, S.; Gladysheva, T.; Valtre, C.; Crenne, J. Y.; Mathieu, M. The crystal structures of TrkA and TrkB suggest key regions for achieving selective inhibition. *J. Mol. Biol.* **2012**, *423* (3), 439–453.
- (14) Oselusi, S. O.; Dube, P.; Odugbemi, A. I.; Akinyede, K. A.; Ilori, T. L.; Egieyeh, E.; Sibuyi, N. R.; Meyer, M.; Madiehe, A. M.; Wyckoff, G. J.; Egieyeh, S. A. The role and potential of computer-aided drug discovery strategies in the discovery of novel antimicrobials. *Comput. Biol. Med.* **2024**, *169*, No. 107927.
- (15) Li, B.; Ma, C.; Zhao, X.; Hu, Z.; Du, T.; Xu, X.; Wang, Z.; Lin, J. YaTCM: Yet another Traditional Chinese Medicine Database for Drug Discovery. *Comput. Struct. Biotechnol. J.* **2018**, *16*, 600–610.
- (16) Pipitò, L.; Illingworth, T. A.; Deganutti, G. Targeting hPKM2 in cancer: A bio isosteric approach for ligand design. *Comput. Biol. Med.* **2023**, *158*, No. 106852.
- (17) Li, B.; Ma, C.; Zhao, X.; Hu, Z.; Du, T.; Xu, X.; Wang, Z.; Lin, J. YaTCM: yet another traditional Chinese medicine database for drug discovery. *Comput. Struct. Biotechnol. J.* **2018**, *16*, 600–610.
- (18) Shadman, Z.; Ghasemali, S.; Farajnia, S.; Mortazavi, M.; Biabangard, A.; Khalili, S.; Rahbarnia, L. In silico Validation of *Pseudomonas aeruginosa* Exotoxin A Domain I Interaction with the Novel Human scFv Antibody. *Infect. Disord.: Drug Targets* **2023**, *23* (5), No. e290323215113.
- (19) Kagami, L.; Wilter, A.; Diaz, A.; Vranken, W. The ACPYPE web server for small-molecule MD topology generation. *Bioinformatics* **2023**, *39* (6), No. btad350, DOI: 10.1093/bioinformatics/btad350.
- (20) da Silva, A. W. S.; Vranken, W. F. ACPYPE - AnteChamber PYthon Parser interface. *BMC Res. Notes* **2012**, *5*, No. 367.
- (21) Lanka, G.; Begum, D.; Banerjee, S.; Adhikari, N.; Yogeewari, P.; Ghosh, B. Pharmacophore-based virtual screening, 3D QSAR, Docking, ADMET, and MD simulation studies: An in silico perspective for the identification of new potential HDAC3 inhibitors. *Comput. Biol. Med.* **2023**, *166*, No. 107481.
- (22) Valdés-Tresanco, M. S.; Valdés-Tresanco, M. E.; Valiente, P. A.; Moreno, E. gmx_MMPBSA: A New Tool to Perform End-State Free Energy Calculations with GROMACS. *J. Chem. Theory Comput.* **2021**, *17* (10), 6281–6291.
- (23) Miller, B. R., 3rd; McGee, T. D., Jr.; Swails, J. M.; Homeyer, N.; Gohlke, H.; Roitberg, A. E. MMPBSA.py: An Efficient Program for End-State Free Energy Calculations. *J. Chem. Theory Comput.* **2012**, *8* (9), 3314–3321.
- (24) Chen, F.; Sun, H.; Wang, J.; Zhu, F.; Liu, H.; Wang, Z.; Lei, T.; Li, Y.; Hou, T. Assessing the performance of MM/PBSA and MM/GBSA methods. 8. Predicting binding free energies and poses of protein-RNA complexes. *RNA* **2018**, *24* (9), 1183–1194.
- (25) Arshia, A. H.; Shadravan, S.; Solhjoo, A.; Sakhteman, A.; Sami, A. De novo design of novel protease inhibitor candidates in the treatment of SARS-CoV-2 using deep learning, docking, and molecular dynamic simulations. *Comput. Biol. Med.* **2021**, *139*, No. 104967.
- (26) Khan, M. F.; Verma, G.; Alam, P.; Akhter, M.; Bakht, M. A.; Hasan, S. M.; Shaquiquzzaman, M.; Alam, M. M. Dibenzepinones, dibenzoxepines and benzosuberones based p38 α MAP kinase inhibitors: Their pharmacophore modelling, 3D-QSAR and docking studies. *Comput. Biol. Med.* **2019**, *110*, 175–185.
- (27) Gosu, V.; Sasidharan, S.; Saudagar, P.; Radhakrishnan, K.; Lee, H. K.; Shin, D. Deciphering the intrinsic dynamics of unphosphorylated IRAK4 kinase bound to type I and type II inhibitors. *Comput. Biol. Med.* **2023**, *160*, No. 106978.
- (28) Chen, J.; Wang, W.; Sun, H.; Pang, L.; Bao, H. Binding mechanism of inhibitors to p38 α MAP kinase deciphered by using multiple replica Gaussian accelerated molecular dynamics and calculations of binding free energies. *Comput. Biol. Med.* **2021**, *134*, No. 104485.
- (29) Wang, T.; Tong, J.; Zhang, X.; Wang, Z.; Xu, L.; Pan, P.; Hou, T. Structure-based virtual screening of novel USP5 inhibitors targeting the zinc finger ubiquitin-binding domain. *Comput. Biol. Med.* **2024**, *174*, No. 108397.
- (30) Jiang, T.; Wang, G.; Liu, Y.; Feng, L.; Wang, M.; Liu, J.; Chen, Y.; Ouyang, L. Development of small-molecule tropomyosin receptor kinase (TRK) inhibitors for NTRK fusion cancers. *Acta Pharm. Sin. B* **2021**, *11* (2), 355–372.
- (31) Timmer, B. J. J.; Mooibroek, T. J. Intermolecular π - π Stacking Interactions Made Visible. *J. Chem. Educ.* **2021**, *98* (2), 540–545.
- (32) Oshita, H.; Shimazaki, Y. π - π Stacking Interaction of Metal Phenoxyl Radical Complexes. *Molecules* **2022**, *27* (3), No. 1135, DOI: 10.3390/molecules27031135.
- (33) Zhu, Y.; Huang, C. X.; Zhang, L.; Wang, Z. F.; Zhao, D. L.; Ding, F.; Zhang, S. Y.; Li, Y. Q.; Chen, L. Z. Promoting the formation of π -stacking interaction to improve CTL cells activation between modified peptide and HLA. *Am. J. Transl. Res.* **2022**, *14* (7), 5164–5177.
- (34) Dai, W.; Jin, P.; Li, X.; Zhao, J.; Lan, Y.; Li, H.; Zheng, L. A carrier-free nano-drug assembled via π - π stacking interaction for the treatment of osteoarthritis. *Biomed. Pharmacother.* **2023**, *164*, No. 114881.